The Promise of Infrared Spectroscopy

Chandrajit Bajaj

Sponsored in part by NIH- R01GM117594, NIH-R41GM116300 and a grant from SETON-Dell Medical 201602388

Computational Visualization Center (CVC) http://cvcweb.ices.utexas.edu
Dept. of Computer Science / Institute for Computational Engineering and Sciences
University of Texas at Austin

Diversity of Infrared Imaging

- Measures scalar intensities (absorbance, reflectance, transmittance, fluorescence,…) across various spectral channels

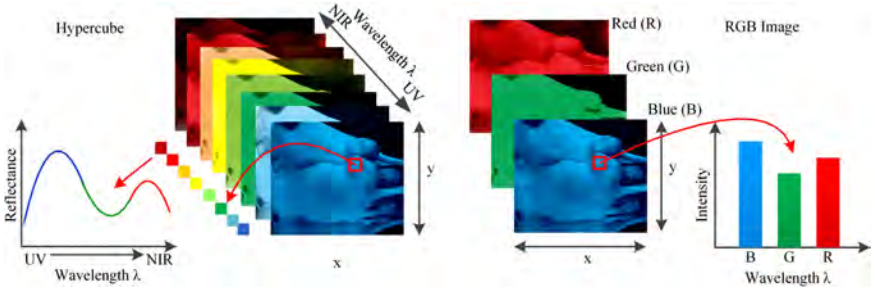

Multispectral Image.

RGB Color Image

Region	Frequency f (THz)	Wavelength λ (μm)	Wavenumber ν (cm^{-1})
Visible	750 — 400	0.4 — 0.7	25000 — 14000
Near IR	400 — 200	0.7 — 1.4	14000 — 7000
SW IR	200 — 120	1.4 — 2.5	7000 — 4000
Mid IR	120 — 12	2.5 — 25	4000 — 400
Far IR	12 — 0.12	25 — 2500	400 — 4

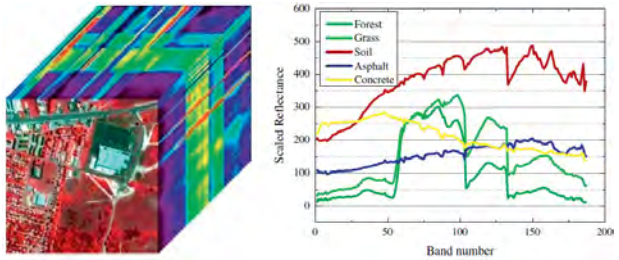

Hydice HYMAP dataset: Resolution 5 m, Size 500 x 500, #Bands 128, Wavelength 0.4 -2.45 um

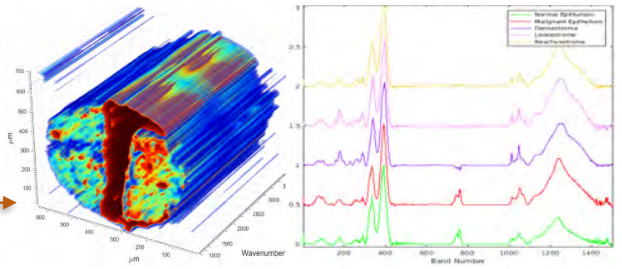

Bottom: BR1003 AGILENT dataset: Resolution 1.1 um, Size 128 x 128, #Bands 1506, Wavelength 2.5 -25 um

Visible vs Mid-Infrared

- Cell/Tissue Classification for Cancer Detection

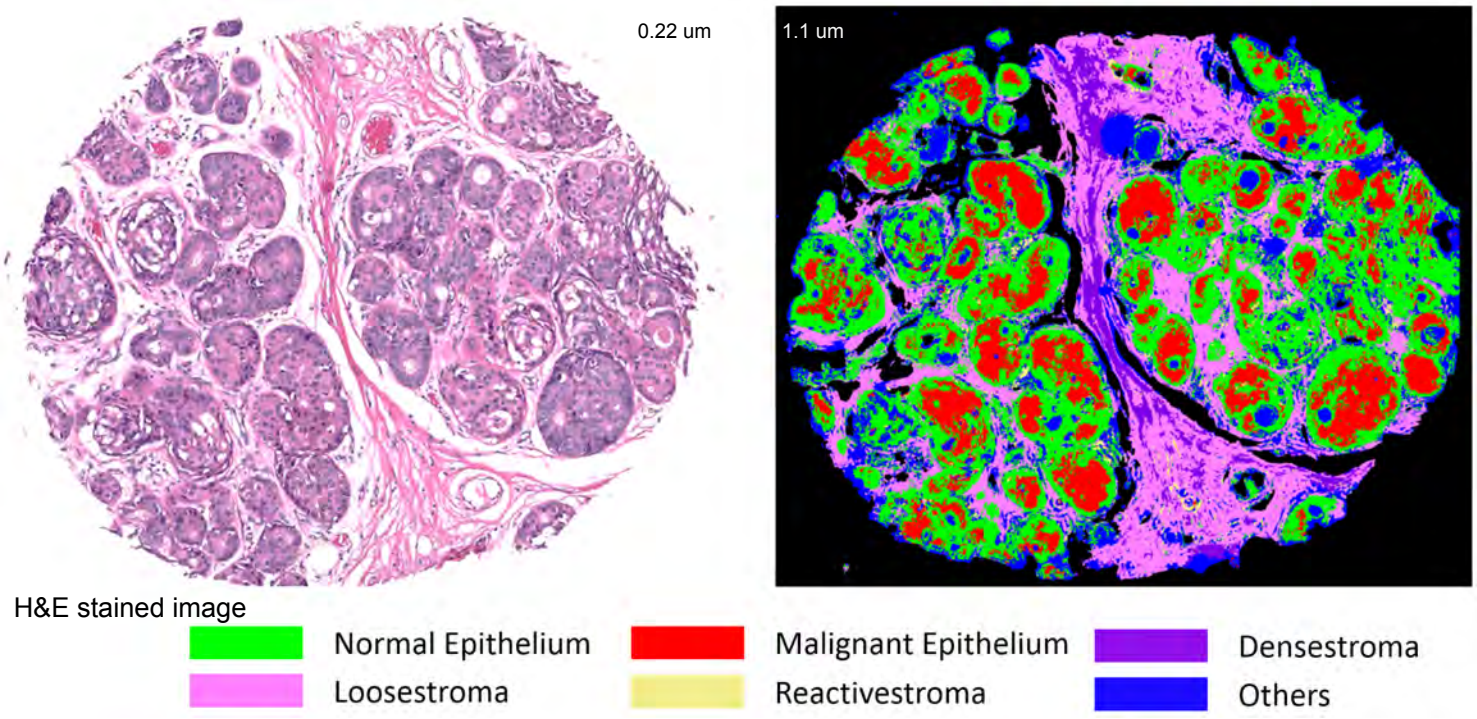

Classified and pathologically verified map of the Tissue Sample: Breast Tissue BR1003,

Tissue (Chemical) Imaging at Cellular Resolution

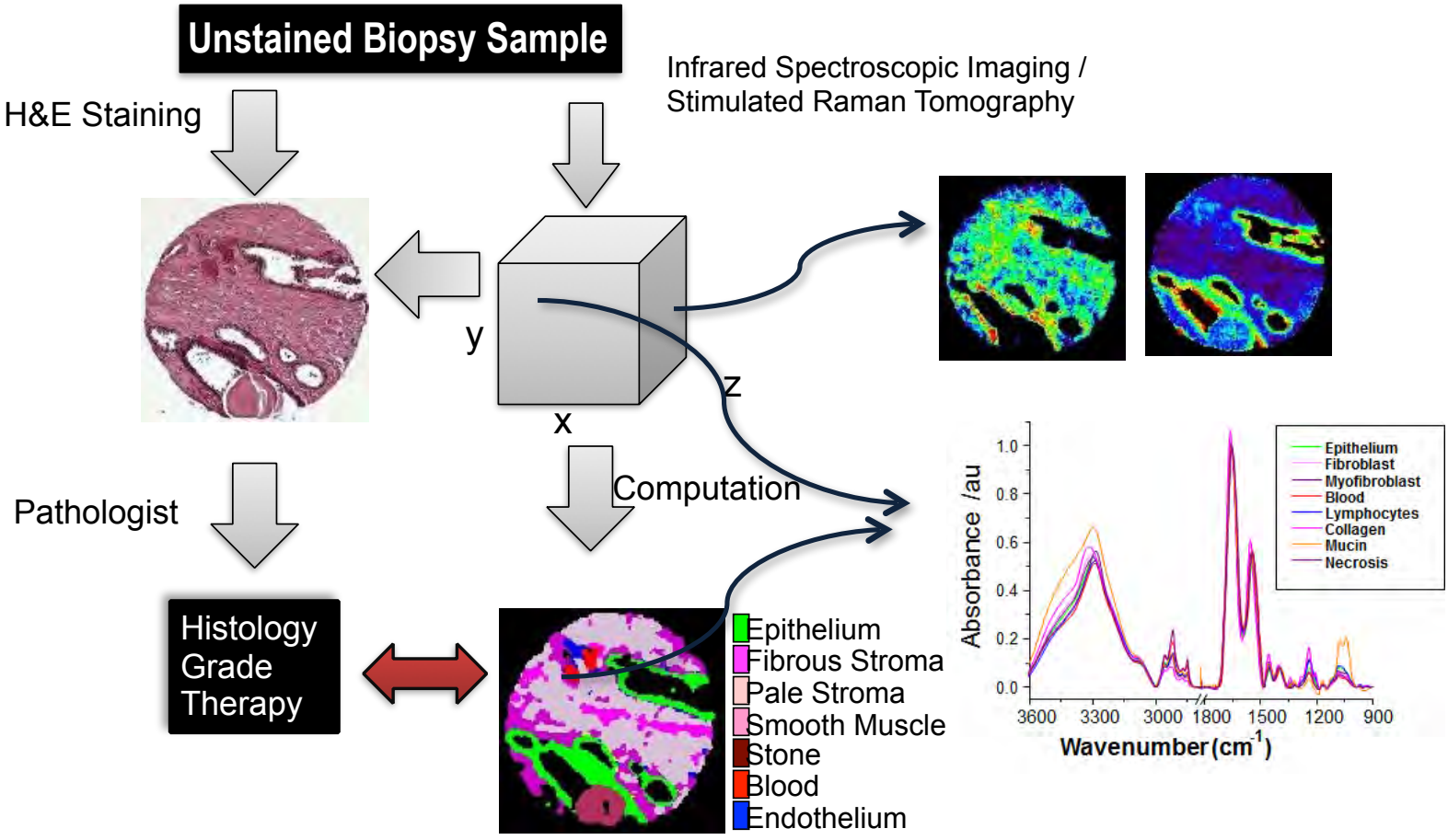

Computational Visualization Center (CVC) http://cvcweb.ices.utexas.edu
Dept. of Computer Science / Institute for Computational Engineering and Sciences
University of Texas at Austin

Small vs Big Data Spectral Analysis

Image Classification / Segmentation

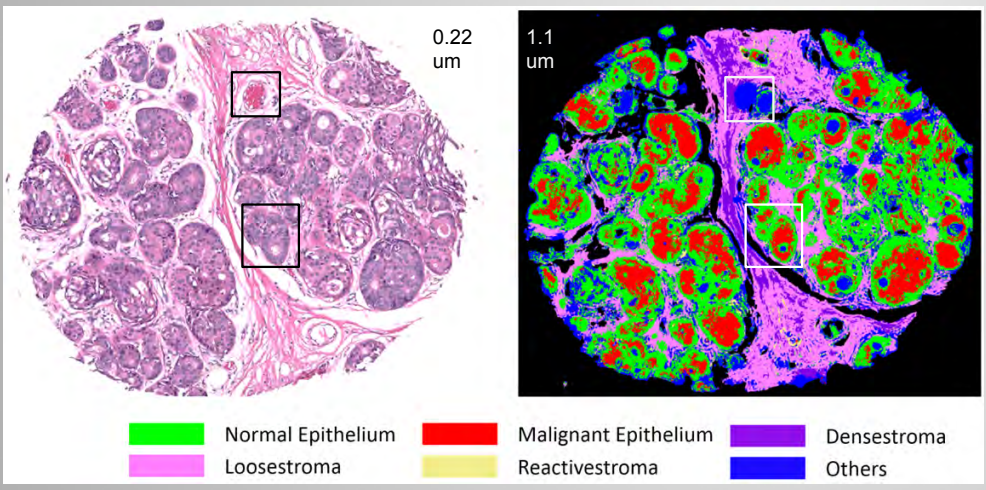

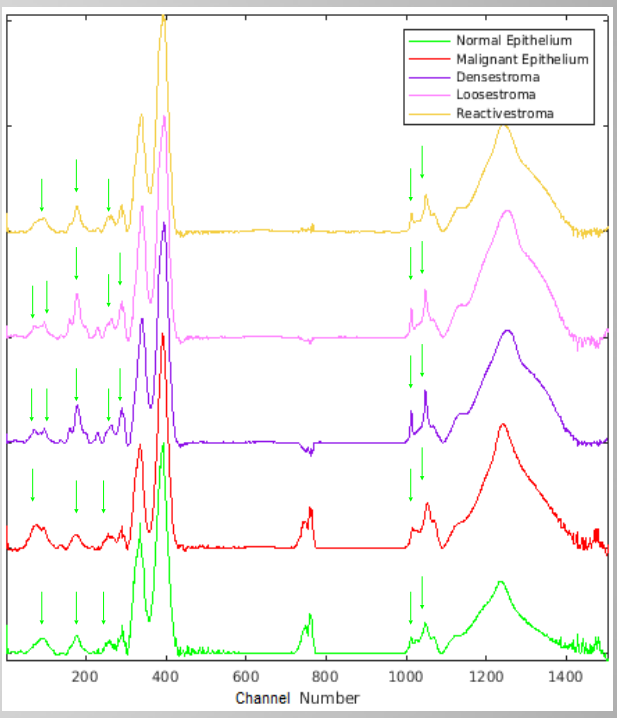

Typical spectra from five different classes of the core

0.005TB/day

1.3TB/day

Need for Noise Estimation and De-Noising

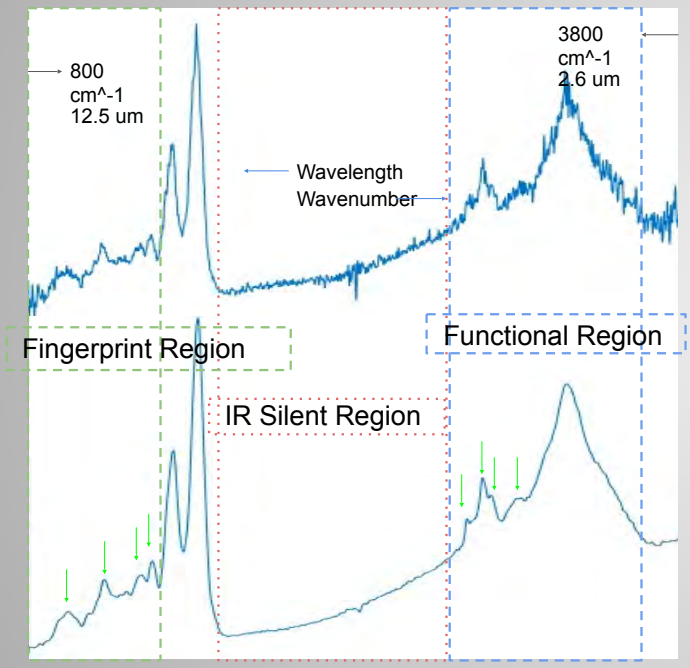

Noisy and DeNoised signal with spectral signature markers

Classification suffers if data is Noisy

- Classifying Malignant Epithelium using Machine Learning
- Denoised Signal: 98-99% correct prediction
- Noisy Signal: 85-86% correct prediction
- Based on well distinguished spectral markers

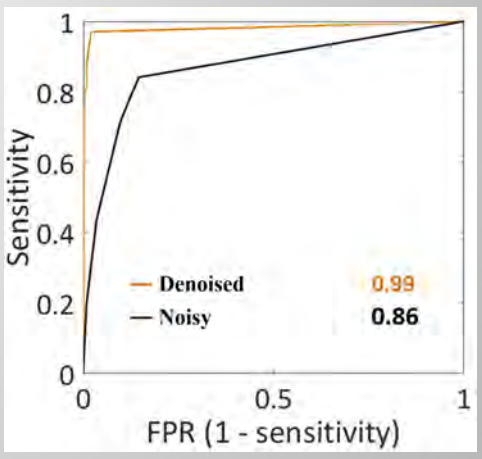

AUC curve for Malignant Epithelium
MNF: (Minimum Noise Fraction) a denoising technique

Combining IR Spectroscopy + Machine Learning

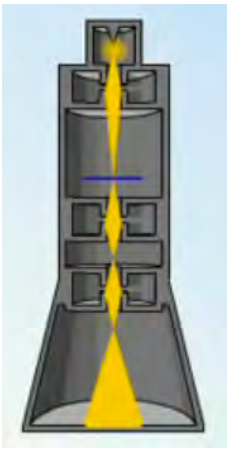

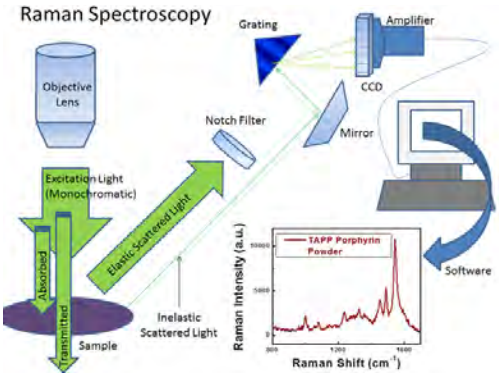

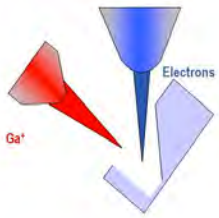

Diagnostic Problem @ Multiple Scales

Current Instrumentation, Uncertainty Analysis…..

Forward Imaging Model

Determine Signal, Noise Dimensionality, Parameter Sensitivity Analysis

Reconstruct Raw Data **Inverse** Model Analysis

Changing the paradigm of data acquisition → modeling → analysis → visualization

Determine Sparsest Data Sampling for S/N and UQ

Augment/Build Instrumentation

Towards Smart Diagnosis
Multi-scale Data Analysis with Quantified Uncertainty

Computational Visualization Center (CVC) http://cvcweb.ices.utexas.edu
Dept. of Computer Science / Institute for Computational Engineering and Sciences
University of Texas at Austin

Noise Estimation: Model and Simulate the Image Acquisition

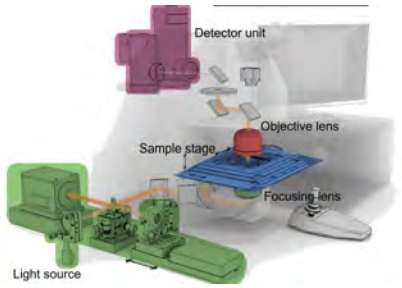

Goal: optimize for image quality

Given a collection Ψ of simulated samples with associated reference images $I_0(x, y, \tilde{\nu}; \mathcal{S})$ and probability distribution $\sum_{\mathcal{S}\in\Psi} p(\mathcal{S}) = 1$, determine the instrument configuration $\hat{\mathbf{c}}$ that gives the "best" expected image

$$\hat{\mathbf{c}} = \arg\min_{\mathbf{c}} \left(\sum_{\mathcal{S}\in\Psi} p(\mathcal{S}) \sum_x \sum_y [I(x, y, \tilde{\nu}; \mathcal{S}, \mathbf{c}) - I_0(x, y, \tilde{\nu}; \mathcal{S})]^2 \right)$$

- Minimize expected deviation from reference image I_0
- Reference samples $\mathcal{S} \in \Psi$ and associated images I_0 supplied by user
- Image function I computed using instrument model
- Using expected difference over collection of samples avoids overfitting
- Choice of sample collection allows optimization for certain types of samples

Computational flow of imaging forward model

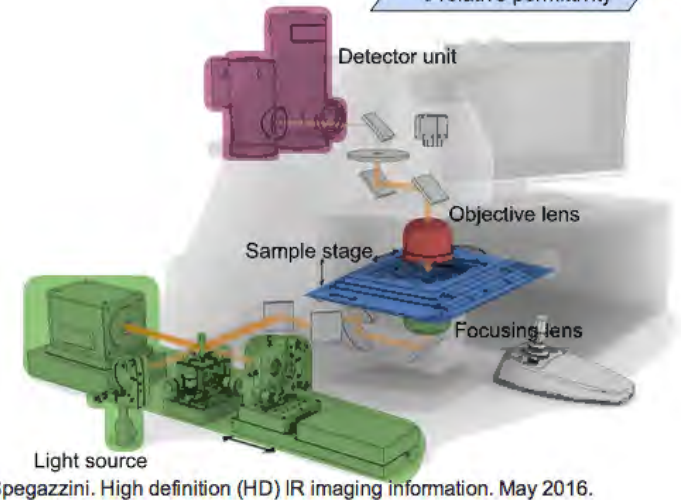

Image: Spegazzini. High definition (HD) IR imaging information. May 2016.

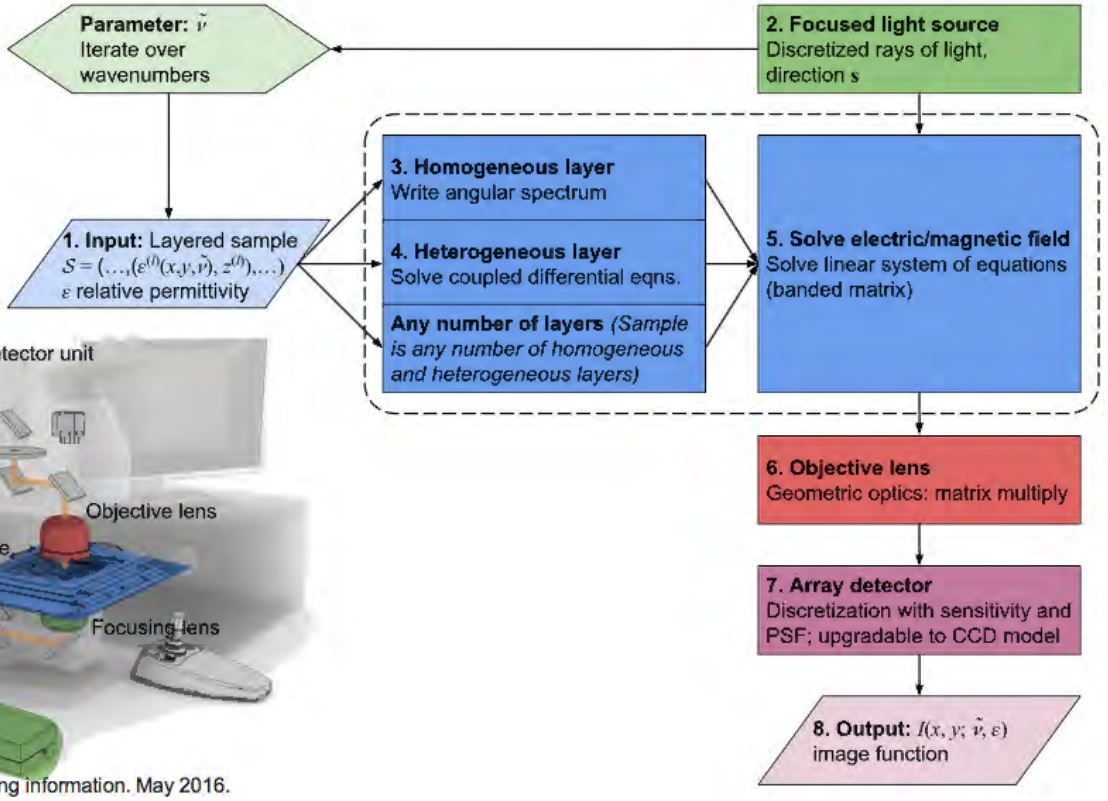

1. Input - Layered sample

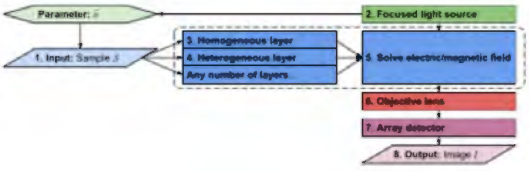

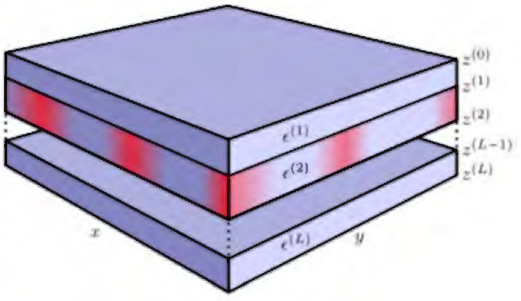

- Model represents sample as layered medium
- Each layer may be modeled either homogeneously or heterogeneously
  - Homogeneous layers: $\epsilon^{(l)}(\tilde{\nu})$ depends only on wavenumber
  - Heterogeneous layers: $\epsilon^{(l)}(x, y, \tilde{\nu})$ depends on x, y position as well
- Variation along the z direction modeled through layers (discretization)
- Sample is described by relative permittivity ϵ — a four-dimensional $(l, x, y, \tilde{\nu})$ complex-valued function — and layer boundary positions $z^{(l)}$
- Sample $\mathcal{S} \approx ((\epsilon^{(1)}, z^{(1)}), (\epsilon^{(2)}, z^{(2)}), \ldots, (\epsilon^{(L)}, z^{(L)}))$

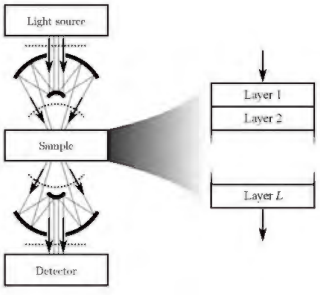

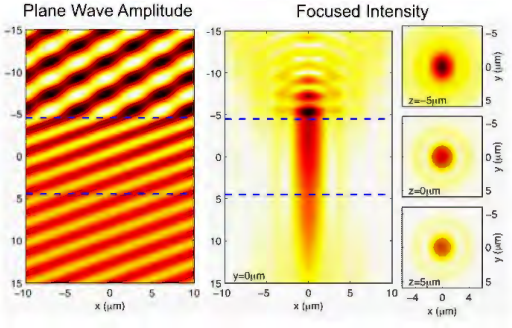

3–5. Light-sample interaction

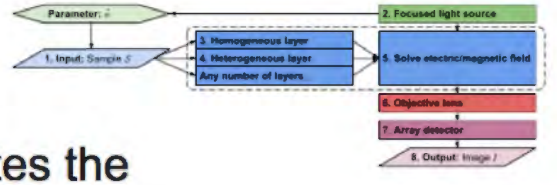

The sample interaction model (steps 3–5) computes the electric and magnetic field in the sample

- Generate constraint equations for each sample layer boundary
  - For homogeneous layers, get constraint equations directly (step 3)
  - For heterogeneous layers, solve differential system first (step 4)
- Solve linear system of $4(L-1)N_F$ equations (step 5) to determine light leaving sample towards detector

$$E_{x,y}^{(l)}(x,y,z^{(l)},\tilde{\nu}) = E_{x,y}^{(l+1)}(x,y,z^{(l)},\tilde{\nu}) \qquad H_{x,y}^{(l)}(x,y,z^{(l)},\tilde{\nu}) = H_{x,y}^{(l+1)}(x,y,z^{(l)},\tilde{\nu})$$

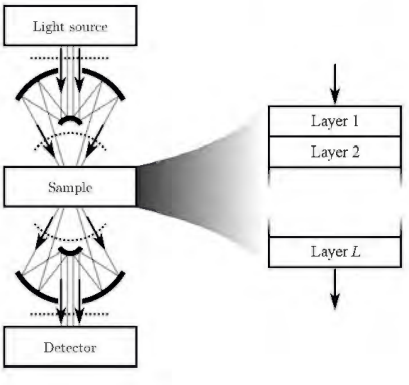

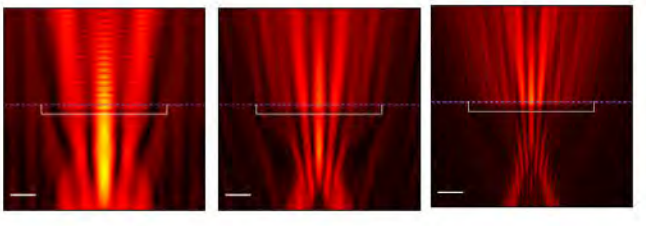

4. Heterogeneous layer computation

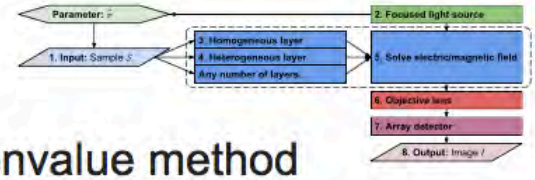

- System of differential equations solved via eigenvalue method

$$\begin{bmatrix} d\mathbf{X}(z,\tilde{\nu})/dz \\ d\mathbf{Y}(z,\tilde{\nu})/dz \\ d\mathbf{I}(z,\tilde{\nu})/dz \\ d\mathbf{J}(z,\tilde{\nu})/dz \end{bmatrix} = i2\pi\tilde{\nu}\Phi(\tilde{\nu}) \begin{bmatrix} \mathbf{X}(z,\tilde{\nu}) \\ \mathbf{Y}(z,\tilde{\nu}) \\ \mathbf{I}(z,\tilde{\nu}) \\ \mathbf{J}(z,\tilde{\nu}) \end{bmatrix}, \qquad \Phi(\tilde{\nu}) = \begin{bmatrix} & & * & * \\ & & * & * \\ * & * & & \\ * & * & & \end{bmatrix} \in \mathbb{C}^{4N_F \times 4N_F}$$

- Block-antidiagonal structure gives eigenvalues in opposite-sign pairs

$$0 = \det(\Phi - \lambda I) = \det \begin{bmatrix} -\lambda I & \Phi_1 \\ \Phi_2 & -\lambda I \end{bmatrix} = \det(\lambda^2 I - \Phi_1 \Phi_2)$$

- Solution is linear combination of eigenvalue pairs, eigenvectors
- Need eigenvalues, eigenvectors returned in opposite-sign pairs, not arbitrary order

Preliminary results: toluene

Top: Simulated by my implementation (solid line), reference implementation (dotted line).
Bottom: Observed spectrum (Coblentz No. 10130).

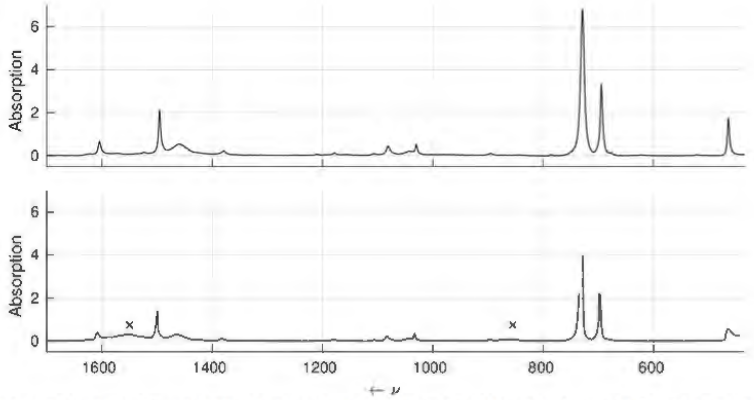

Coblentz Society, Inc. Evaluated infrared reference spectra. In Linstrom and Mallard, editors, *NIST Chemistry WebBook, NIST Standard Reference Database Number 69*. Gaithersburg MD, 20899. Accessed 30 May 2017.
SDBS No. 97. In *SDBSWeb: Spectral Database for Organic Compounds*. National Institute of Advanced Industrial Science and Technology, Tokyo. Accessed 5 June 2017.

Preliminary results: hexane

Top: output from my implementation (solid line), reference implementation (dotted line).
Bottom: Observed spectrum (Coblentz No. 10118).

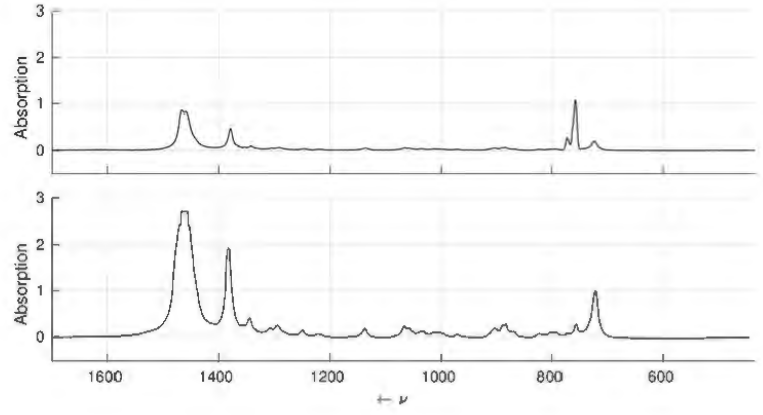

Coblentz Society, Inc. Evaluated infrared reference spectra. In Linstrom and Mallard, editors, *NIST Chemistry WebBook, NIST Standard Reference Database Number 69*. Gaithersburg MD, 20899. Accessed 30 May 2017.

The Spectral De-Noising Problem

Given Noisy data (Y = D + ε) under an unknown noise model ε, obtain an approximation $\bar{D}$:

1. Maximize the Signal to Noise Ratio (SNR) $\bar{D} = \underset{D}{argmax} \frac{var(D)}{var(\epsilon)}$
2. Preserve structural details in the image domain
3. Preserve spectral markers F (peak position, peak location, relative peak spacing) $F = [j, L] \quad j \in [1 : S], L \in \{0, 1\}$

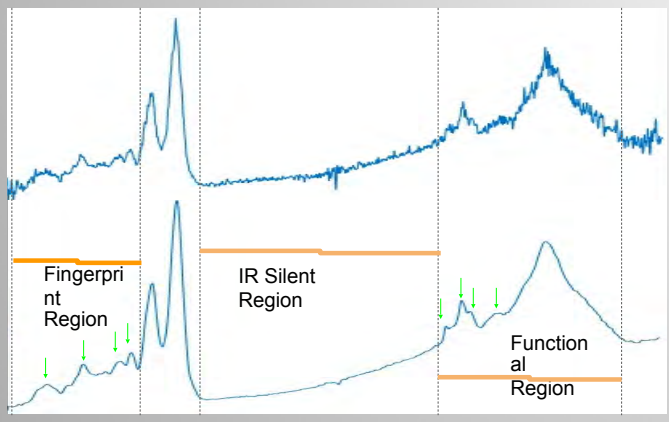

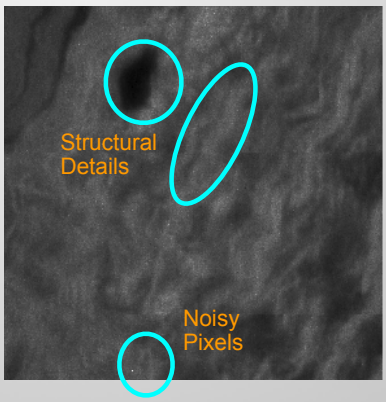

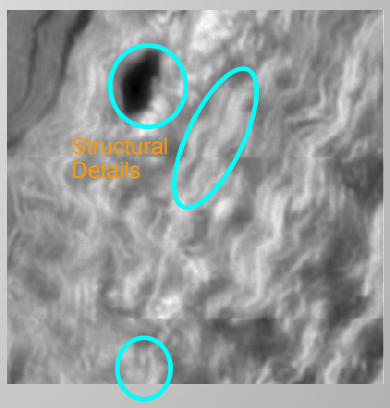

Metrics for De-Noising evaluation

- Spatial
  a. Classification Accuracy
- Spectral
  a. Preservation of spectral features
  b. Spatial profile analysis

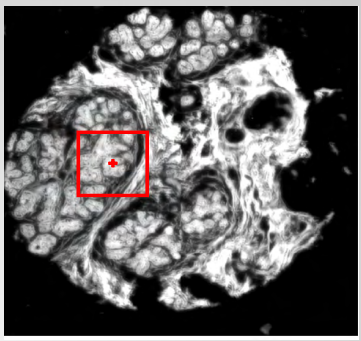

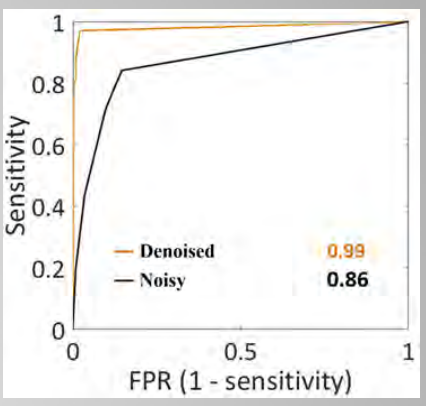

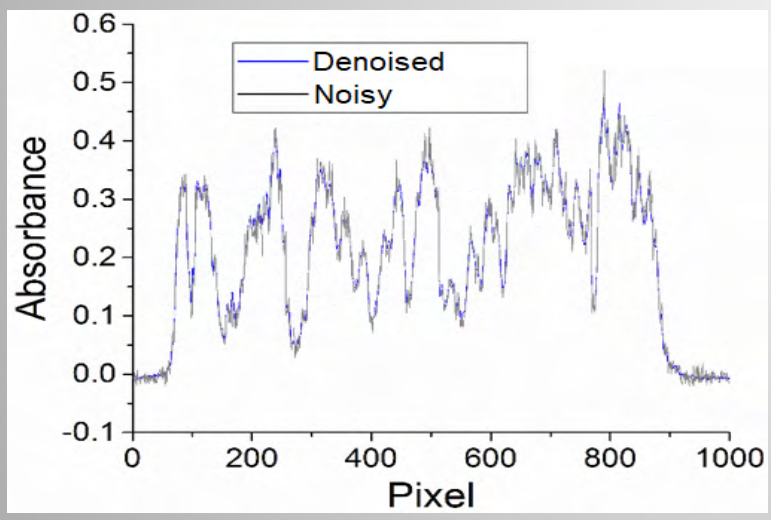

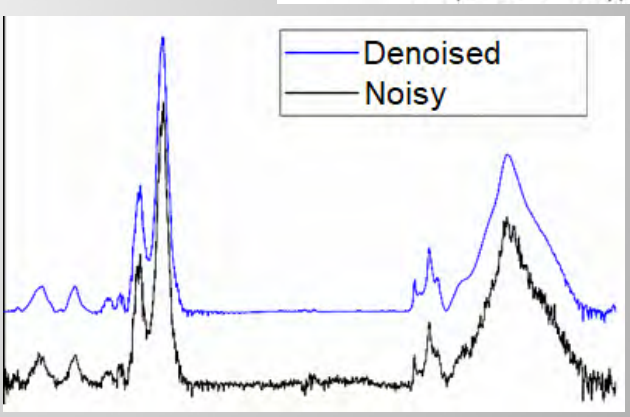

Challenges for De-Noising in Mid IR

- Most algorithms fail if the data is noisy
- Spectral markers get corrupted or lost
- Signal and noise maybe correlated
- Noise correlated across multiple channels*

$$\epsilon_s \sim= \rho \cdot \epsilon_{s-1} + \epsilon, \epsilon \sim \mathcal{N}(\mu, \sigma^2)$$

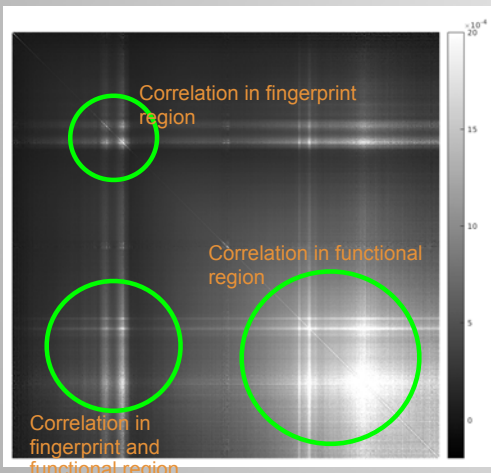

Covariance matrix of approximated noise in the FTIR data

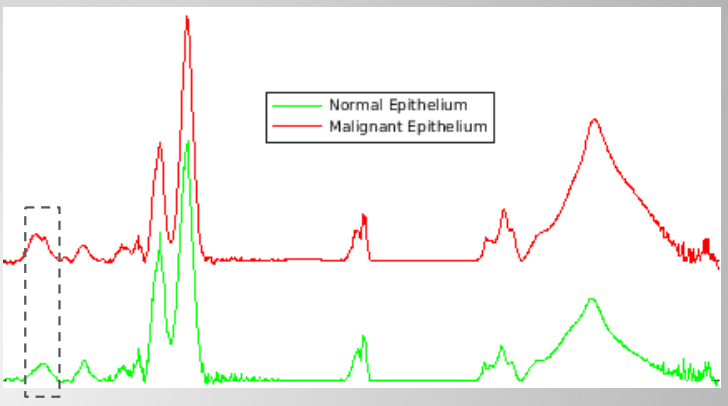

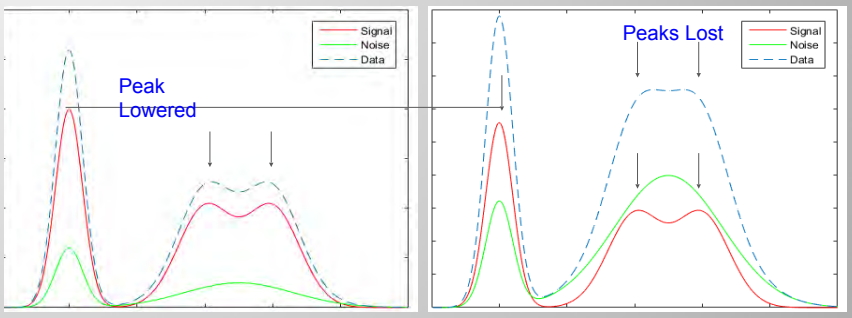

Illustration when noise is correlated within channels and also to data

* Leger et al. "Methods for systematic investigation of measurement error covariance matrices." *Chemometrics and Intelligent Laboratory Systems* 77.1 (2005): 181-205.

Prior De-Noising Techniques

- Filtering based approaches on spectrum *$+
- Coefficients chosen by human experimentation
- Can handle any kind of noise
- Initial analysis is very time consuming
- Recalculate for every new dataset
- Good Classification accuracy

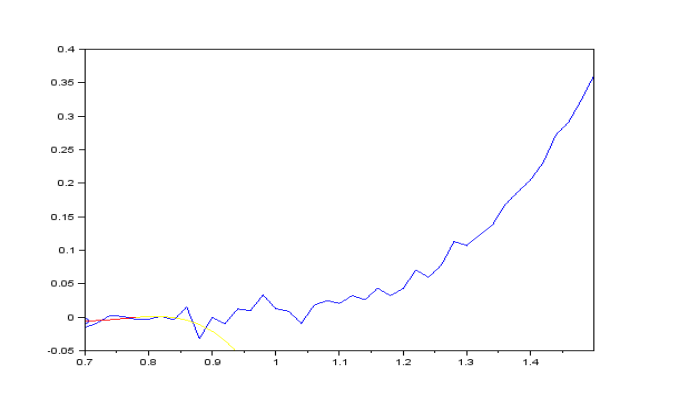

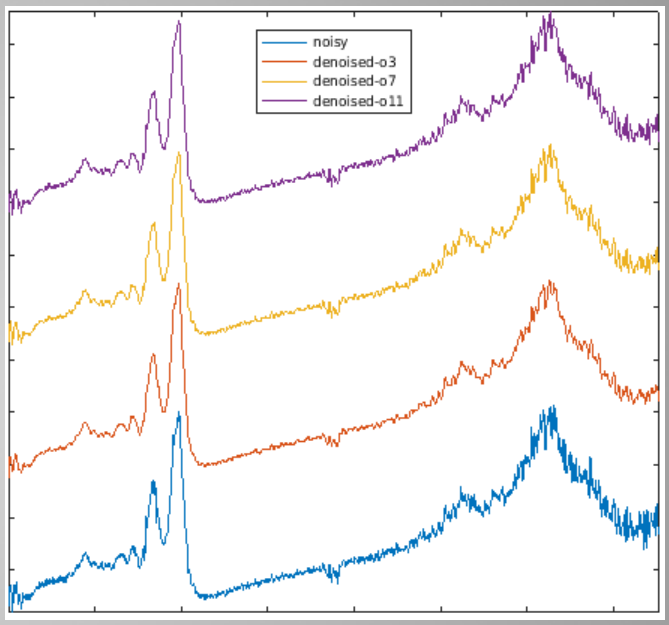

Results of Savitzky Golay filtering with different order polynomial fitting

* Savitzky, Abraham, and Marcel JE Golay. "Smoothing and differentiation of data by simplified least squares procedures." Analytical chemistry 36.8 (1964): 1627-1639.
$ Kawata, Satoshi, and Shigeo Minami. "Adaptive smoothing of spectroscopic data by a linear mean-square estimation." Applied spectroscopy 38.1 (1984): 49-58.
+ Tsai, Fuan, and William Philpot. "Derivative analysis of hyperspectral data." Remote Sensing of Environment 66.1 (1998): 41-51.

Prior De-Noising Techniques

- Signal is much stronger than noise
  - Signal and noise are independent
  - Noise across channels are independent
- Recover a low rank structure from the data where all the major signal contributions lie, and with with sparse noise structure *+
- Perform multi-modal Iteration using Parallel Factor Analysis or Multidimensional Weiner based filters on the HSI cube $%
- Use a rank-1 approximated tensor decomposition approach #
- Model the signal and noise as gaussian random fields and solve using Bayesian approach &

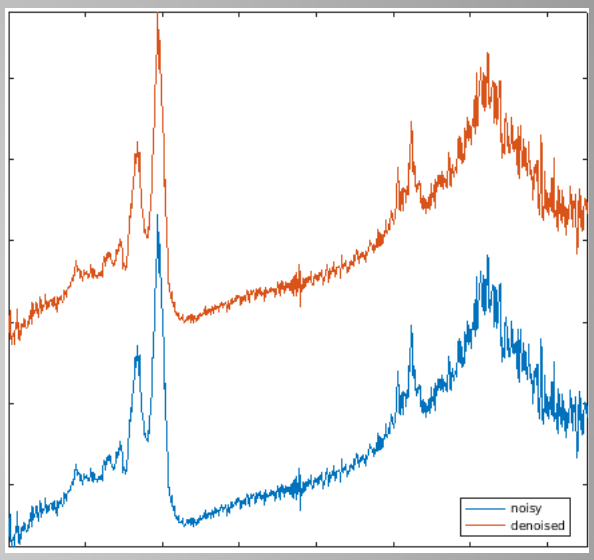

Assumption on independent noise model results in negligible denoising

$$\delta_i = \exp(-c\Sigma_\delta(i,i))$$

* Zhang et al. "Hyperspectral image restoration using low-rank matrix recovery." IEEE Transactions on Geoscience and Remote Sensing 52.8 (2014): 4729-4743

+ Wei, et al. "Hyperspectral image denoising via noise-adjusted iterative low-rank matrix approximation." IEEE Journal of Selected Topics in Applied Earth Observations and Remote Sensing 8.6 (2015): 3050-3061

$ Xuefeng et al. "Reduction of signal-dependent noise from hyperspectral images for target detection." IEEE Transactions on Geoscience and Remote Sensing 52.9 (2014): 5396-5411

% Letexier, Damien, and Salah Bourennane. "Noise removal from hyperspectral images by multidimensional Filtering." IEEE Transactions on Geoscience and Remote Sensing 46.7 (2008): 2061-2069

Guo, Xian, et al. "Hyperspectral image noise reduction based on rank-1 tensor decomposition." *ISPRS journal of photogrammetry and remote sensing* 83 (2013): 50-63.

& Zhong et al. "Jointly learning the hybrid CRF and MLR model for simultaneous denoising and classification of hyperspectral imagery." *IEEE Transactions on Neural Networks and Learning Systems* 25.7 (2014): 1319-1334

Minimum Noise Fraction (MNF)

- Developed by Green et al. *
- Can handle cases when signal and noise are uncorrelated
- Noise can be correlated within channels
- Orders data in terms of SNR in the MNF transformed space

Algorithm 1 MNF($Y \in \mathbb{R}^{N \times S}$)

1: Estimate Data Covariance Matrix: $\Sigma_Y = Cov\{Y\}$
2: If δ is unknown, estimate: $\delta \sim Y(j,:) - Y(j+1,:), \forall j = 1 : N-1$
3: Estimate Noise Covariance Matrix: $\Sigma_\delta = \frac{1}{2} Cov\{\delta\}$
4: Calculate MNF projection vectors: $(\Sigma_Y \Sigma_\delta^{-1})\Phi = \Lambda_{MNF}\Phi$
5: Project data along MNF vectors: $Y_{MNF} \in \mathbb{R}^{N \times S} = Y\Phi$
6: Initialize $R \in \mathbb{R}^{S \times S}$ as top rank-K matrix
7: Project data back: $\bar{D} \in \mathbb{R}^{N \times S} = Y_{MNF} R(\Phi^{-1}) = Y\Phi R(\Phi^{-1})$

* Green, Andrew A., et al. "A transformation for ordering multispectral data in terms of image quality with implications for noise removal." IEEE Transactions on geoscience and remote sensing 26.1 (1988): 65-74

Minimum Noise Fraction: Geometry

$$\Sigma_Y = \Sigma_D + \Sigma_\delta$$ Data Covariance Structure

$$\Sigma_\delta = E\Lambda E^T$$ Spectral Decomposition of Noise Covariance

$$\begin{aligned}\Sigma_W &= (E\Lambda_\delta^{-1/2})^T \Sigma_Y (E\Lambda_\delta^{-1/2}) \\ &= (E\Lambda_\delta^{-1/2})^T \Sigma_D (E\Lambda_\delta^{-1/2}) + (E\Lambda_\delta^{-1/2})^T \Sigma_\delta (E\Lambda_\delta^{-1/2}) \\ &= \Sigma_{W(D)} + I_\delta \quad \text{Whitened Noise Covariance} \\ \Sigma_W &= G\Lambda_{MNF} G^T \quad \text{Spectral Decomposition of Whitened Data}\end{aligned}$$

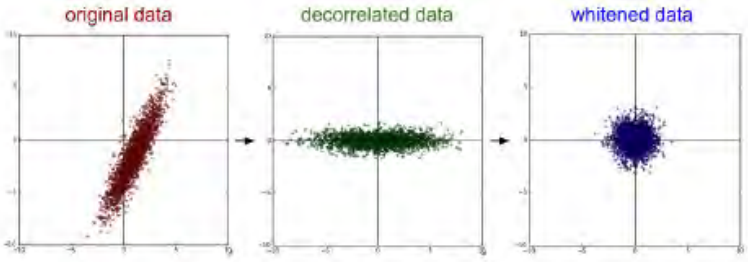

Figure: Geometric Interpretation of Whitening. Left: Orientation of noise. Middle: Orientation of noise after multiplication with E. Right: Orientation of noise after multiplication with $\Lambda_\delta^{-1/2}$

Minimum Noise Fraction: Fast MNF

$$
\begin{aligned}
D &= Y * \Phi * R * \Phi^{-1} \\
&= Y * (E * \Lambda_\delta^{-1/2} * G) * R * (E * \Lambda_\delta^{-1/2} * G)^{-1} \\
&= Y * E * \Lambda_\delta^{-1/2} * G * R * G^T * \Lambda_\delta^{1/2} * E^T \\
&= Y * E * \Lambda_\delta^{-1/2} * G * R * R^T * G^T * \Lambda_\delta^{1/2} * E^T \\
&= Y * \hat{\Phi} * \tilde{\Phi}^T \; //fastMNF \\
\Rightarrow R &= \left[\begin{array}{c|c} I_K & 0 \\ \hline 0 & 0 \end{array}\right] \\
\Rightarrow \hat{\Phi} &= E * \Lambda_\delta^{-1/2} * G * R \qquad //\text{forward MNF transform} \\
\Rightarrow \tilde{\Phi} &= E * \Lambda_\delta^{1/2} * G * R \qquad //\text{inverse MNF transform}
\end{aligned}
$$

Algorithm 1 MNF($Y \in \mathbb{R}^{N \times S}$)

1: Estimate Data Covariance Matrix: $\Sigma_Y = Cov\{Y\}$
2: If δ is unknown, estimate: $\delta \sim Y(j,:) - Y(j+1,:), \forall j = 1 : N-1$
3: Estimate Noise Covariance Matrix: $\Sigma_\delta = \frac{1}{2} Cov\{\delta\}$
4: Calculate MNF projection vectors: $(\Sigma_Y \Sigma_\delta^{-1})\Phi = \Lambda_{MNF}\Phi$
5: Project data along MNF vectors: $Y_{MNF} \in \mathbb{R}^{N \times S} = Y\Phi$
6: Initialize $R \in \mathbb{R}^{S \times S}$ as top rank-K matrix
7: Project data back: $\tilde{D} \in \mathbb{R}^{N \times S} = Y_{MNF} R(\Phi^{-1}) = Y\Phi R(\Phi^{-1})$

- Previously slow due to inversion of large matrices
- Current formulation avoids any inverse
- Uses rank-K approximation of G

Variations on Minimum Noise Fraction: Fast MNF

Approx MNF

Rand MNF

- Block Lanczos [#] method to compute a rank K' SVD
- Guarantees (1+ε) Frobenius and (1+ε) spectral norm approximation
- Guarantees ε per vector norm approximation
- Although the Block Lanczos algorithm can attain machine precision
- Block Lanczos is rel.slow when the matrix is large
- A faster randomized and memory efficient version [&]
- Computes the K'-SVD up to (1+ε) Frobenius norm relative error
- Only keeps a N x O(K'/ε) sketch in memory

[$] Musco, Cameron, and Christopher Musco. "Stronger approximate singular value decomposition via the block lanczos and power methods." Advances in Neural Information Processing Systems (NIPS) (2015).

[&] Halko, Nathan, Per-Gunnar Martinsson, and Joel A. Tropp. "Finding structure with randomness: Probabilistic algorithms for constructing approximate matrix decompositions." SIAM review 53.2 (2011): 217-288.

Algorithm	Time	Space
1. MNF	$\mathcal{O}(S^3 + NS^2)$	$\mathcal{O}(NS + S^2)$
2. Fast MNF	$\mathcal{O}(S^3 + NSK)$	$\mathcal{O}(NK + S^2)$
3. Approx MNF	$\mathcal{O}(S^2K + NSK)$	$\mathcal{O}(NK + SK)$
4. Rand MNF	$\mathcal{O}(nnz(\Sigma_W)K + NSK)$	$\mathcal{O}(NK + SK)$

Table: Comparison of Time and Space complexity of MNF versions. $\mathcal{O}$: big-O complexity. $nnz(X)$: #non-zero elements in X. N: # pixels, S: # spectral bands and K: # chosen bands.

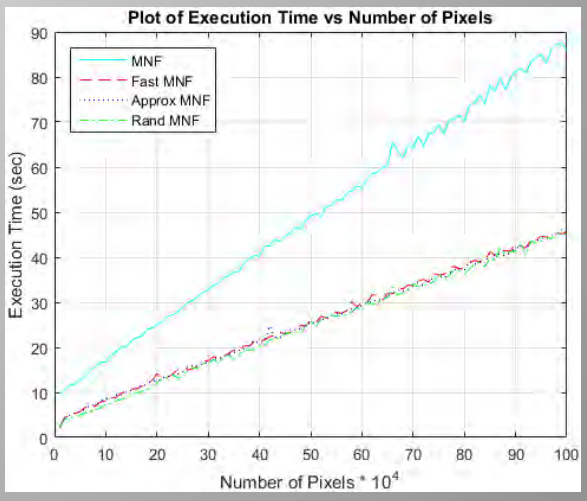

Minimum Noise Fraction: Profile Analysis

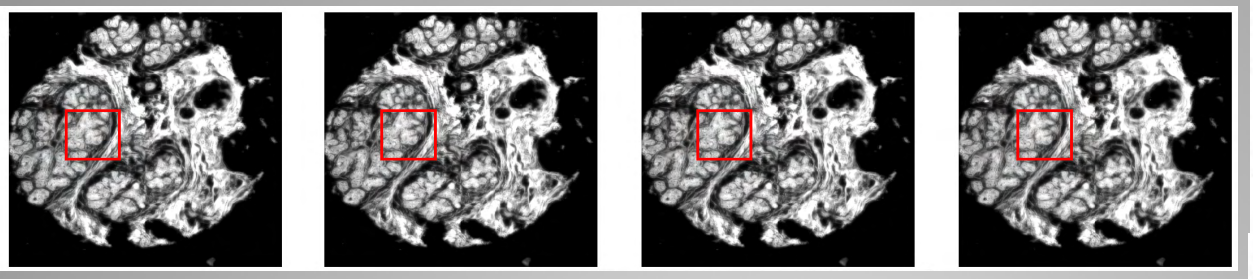

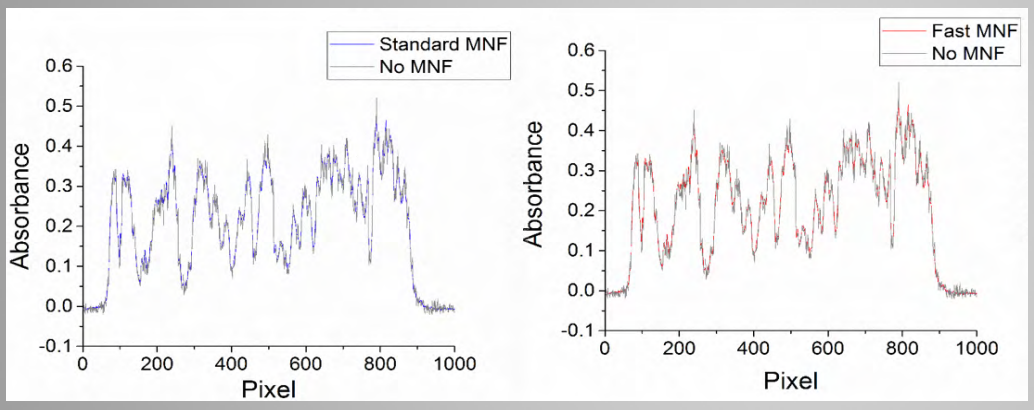

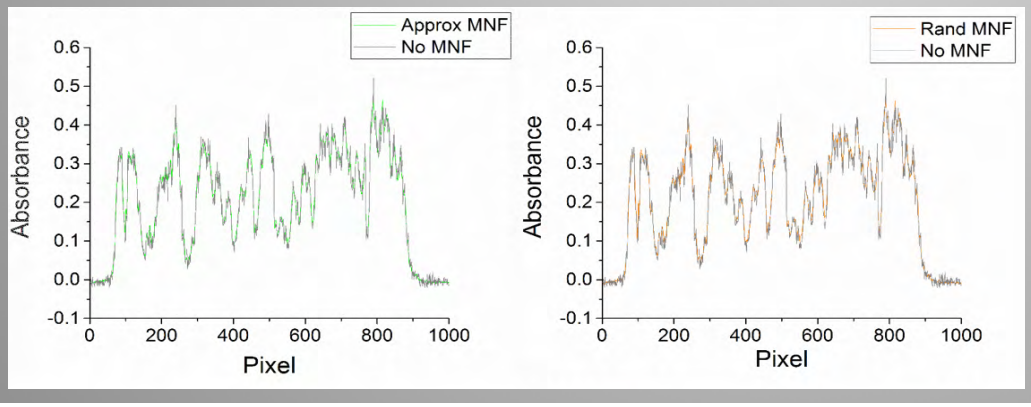

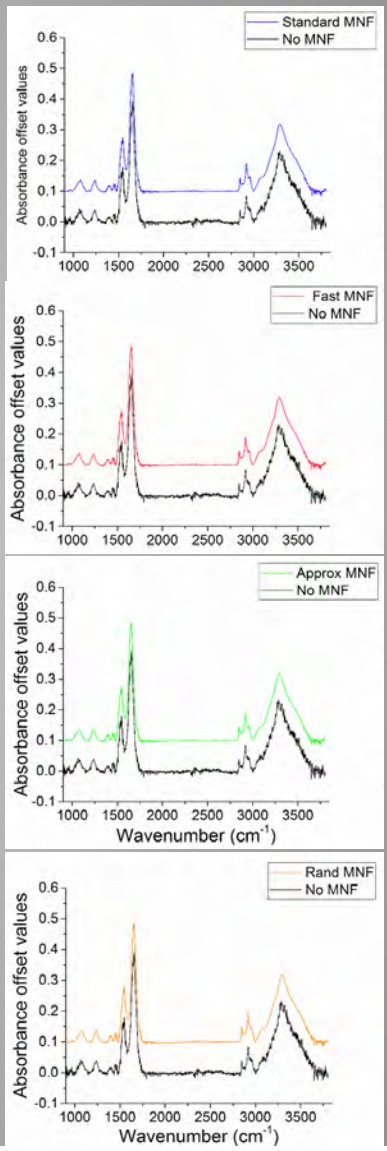

Minimum Noise Fraction: Classification Analysis

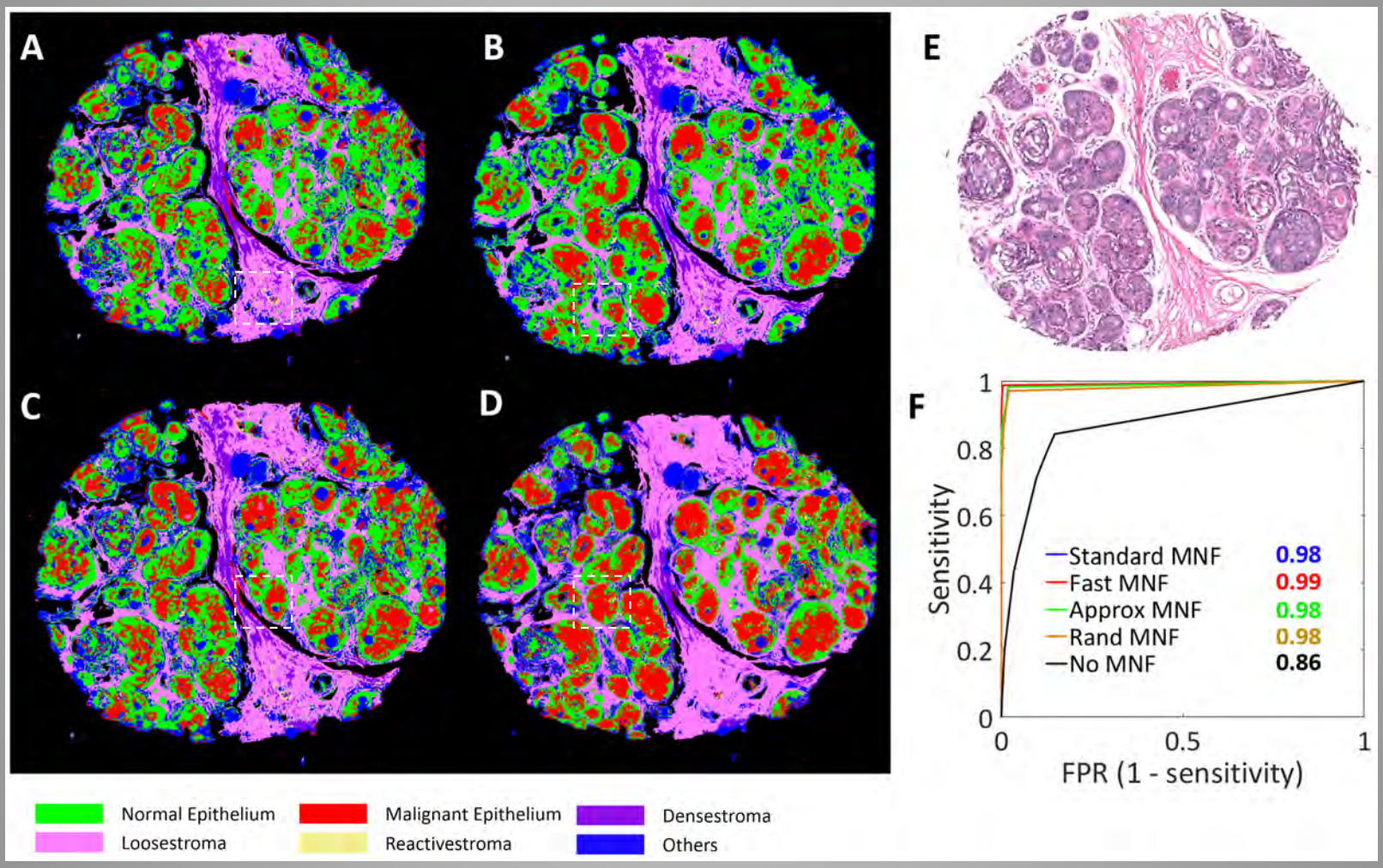

Next Steps: Super-Resolution IR

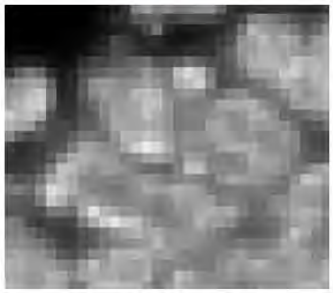

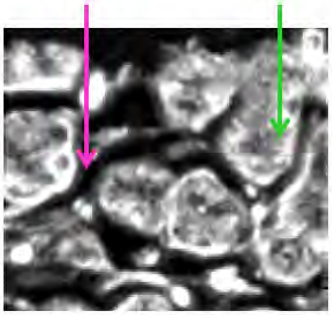

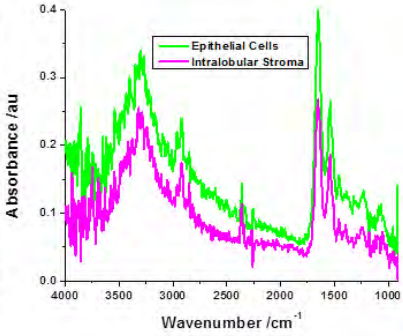

Breast Tissue

Visualization and chemical characterization of intralobular stroma.

Globar 15X FT-IR

Globar 74X FT-IR

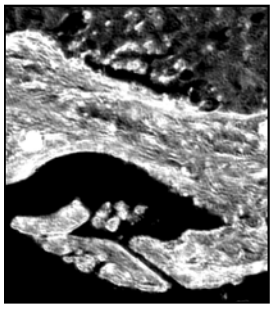

ProstateTissue

Visualization and chemical characterization of collagen bands

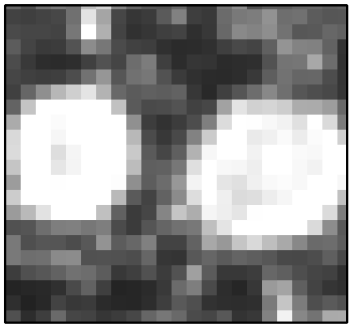

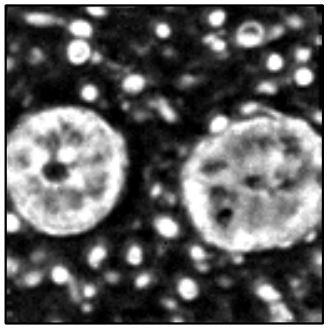

Colon Tissue

Visualization and chemical characterization of subcellular mucin

Computational Visualization Center (CVC) http://cvcweb.ices.utexas.edu
Dept. of Computer Science / Institute for Computational Engineering and Sciences
University of Texas at Austin

Nasse et al. *Nature Methods* (2011);
Reddy et al *Appl Spectrosc* (2013)

Collaboration with Rohit Bhargava, UIUC

Next Steps: Tunable Quantum Cascade Laser

(Compressed Sensing)

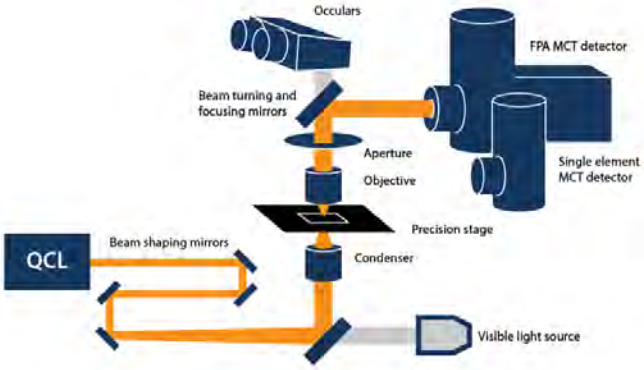

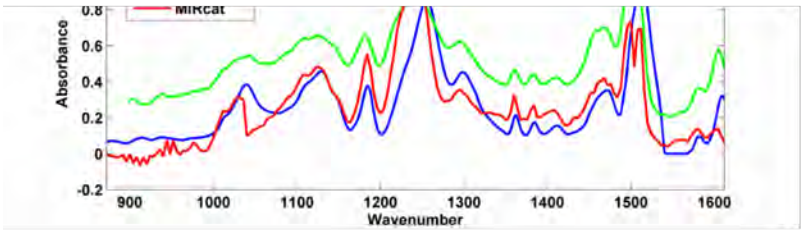

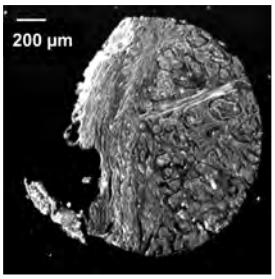

Frontier – Imaging with QCLs

- Excellent SNR (10^4); 10^5 pix/$s.\Delta\nu$
- Ideal for ML approaches → use discrete frequency data for classification
- Limited frequency range

SMART DATA ANALYSIS: Tumor Cytotyping, Tracking Progression in 3D with Molecular-Cell Precision

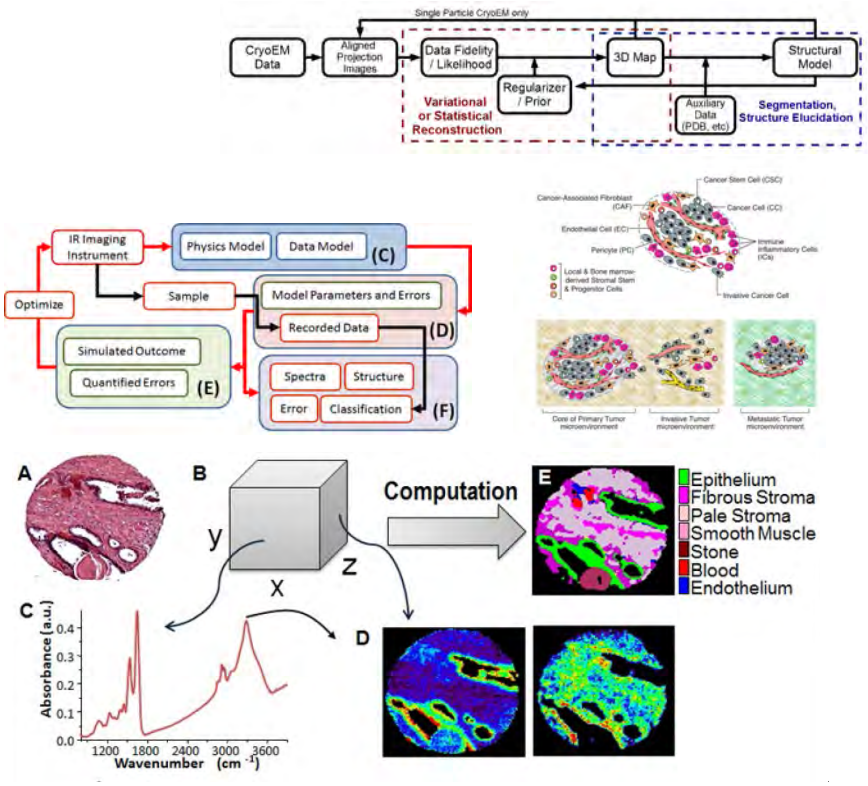

(D) nucleic acids (left, at 1080cm^{-1}) and collagen specific (right, at 1245cm^{-1}).

Developing computational tools convert chemical imaging data to knowledge, as shown here for identifying all cells in prostate tissue (E).

Learning the Heterogeneity in cellular morphology, with a reduction in cell polarity during branching morphogenesis

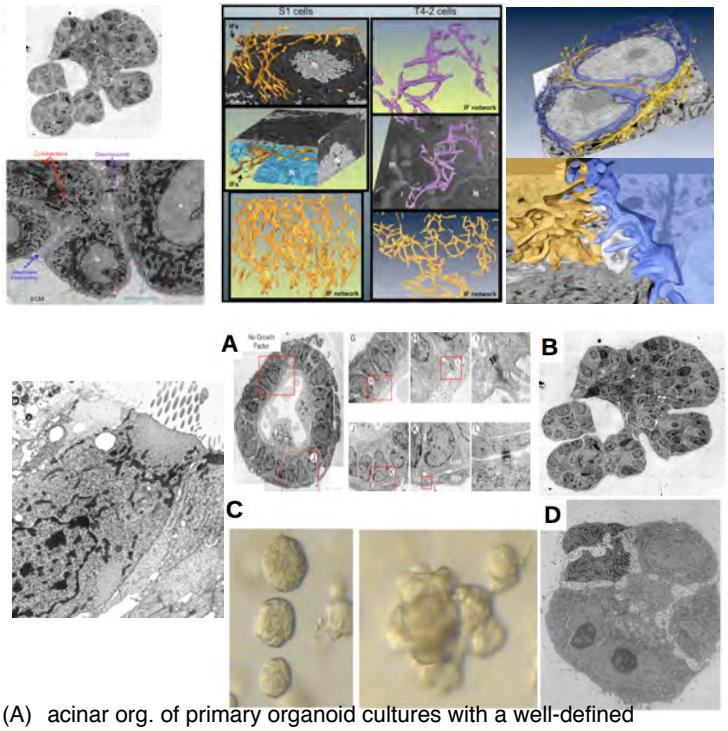

(A) acinar org. of primary organoid cultures with a well-defined lumen
(B) 200 micron x 200 micron field of view of a single 100 nm thin resin section imaged at 1 nm resolution of an organoid undergoing branching morphogenesis
(C) HMT-3522 S1 acini (left) and T4 aggregates (right).
(D) S1 cells form growth-arrested acini with extensive intercellular membrane network and reduction in cell polarity, illustrating the label-free resolving power of the electron microscope.

DETAILS

Sources for hyperspectral images

- Airborne Visible/Infrared Imaging Spectrometer (AVIRIS) program
  - Spatial resolution 20 meters at 20 km altitude, 4 meters at 4 km
  - 0.4-2.5 μm
- Advanced Spaceborne Thermal Emission and Reflection Radiometer (ASTER) Spectral Library
  - 2000 spectra of minerals, rocks, soils, water
  - 0.4-14 μm
- USGS Spectral Library
  - 500 spectra of minerals and a few plants
  - 0.2-3.0 μm

Reflectance vs. radiance

Laboratory instruments observe reflectance (or absorption), while remote sensing observes radiance, capturing several effects which must be corrected for.

- Spectrum of illuminating (solar) light
  - Additionally affected by shadows
- Light interactions with atmosphere
  - e.g. absorbance by water vapor, CO_2
- Illumination geometry (angle of incidence)
  - Varies by time of day and season
- Sensor characteristics
  - Variations between sensors, temporal changes

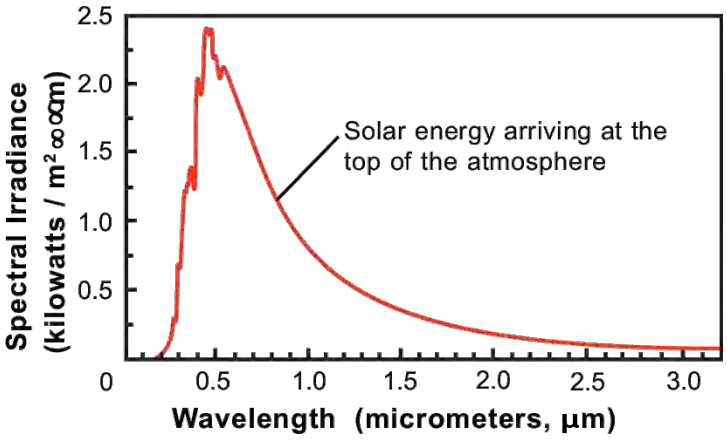

Hyperspectral image acquisition

- Imaging spectrometers capture hyperspectral images
- Remote sensing
  - Analysis of the surface of the Earth (or other planets)
  - Optical dispersing element to separate frequencies
  - Can have spectral resolution as fine as 0.01 μm
  - Broadband (solar) light source
- Hyperspectral images also used in microscopy
  - Focal plane array detector
  - FTIR spectroscopy using interferometer light source

Hyperspectral instrument specifications

	AVIRIS	ASTER	Agilent Cary FTIR	QCL DFIR
Image size	677 pixels wide	4980 pixels wide (V/NIR)	128 × 128 pixels	128 × 128 pixels
Spatial resolution	20m (at 20km alt.) 4m (at 4km alt.)	15m (V/NIR) 30m (SWIR) 90m (MidIR)	1.1 μm	0.95 μm
Spectral resolution	0.01 μm in 0.4-2.5 μm	14 bands increments of 0.4-14 μm	0.0002 μm increments of 1.1-28.5 μm	0.002 μm in 5.25-12.87 μm
Detector	Si (Vis) InGaAr (NIR) InSb (SWIR)	Si (V/NIR) PtSi-Si (SWIR) HgCdTe (MidIR)	DLaTGS or HgCdTe (MCT)	HgCdTe (MCT)
SNR	100 (at 0.49	varies	10,000	260 (single

Research and commercial imaging spectrometers

Sensor	Organization	Country	# bands	Wavelengths
AVIRIS	NASA	United States	224	0.4 - 2.5 µm
AISA	Spectral Imaging Ltd	Finland	286	0.45 - 0.9 µm
CASI	Itres Research	Canada	288	0.43 - 0.87 µm
DAIS 2115	GER Corp	United States	211	0.4 - 12.0 µm
HYMAP	Integrated Spectronics Pty Ltd	Australia	128	0.4 - 2.45 µm
PROBE	Earth Search Sciences	United	128	0.4 - 2.45

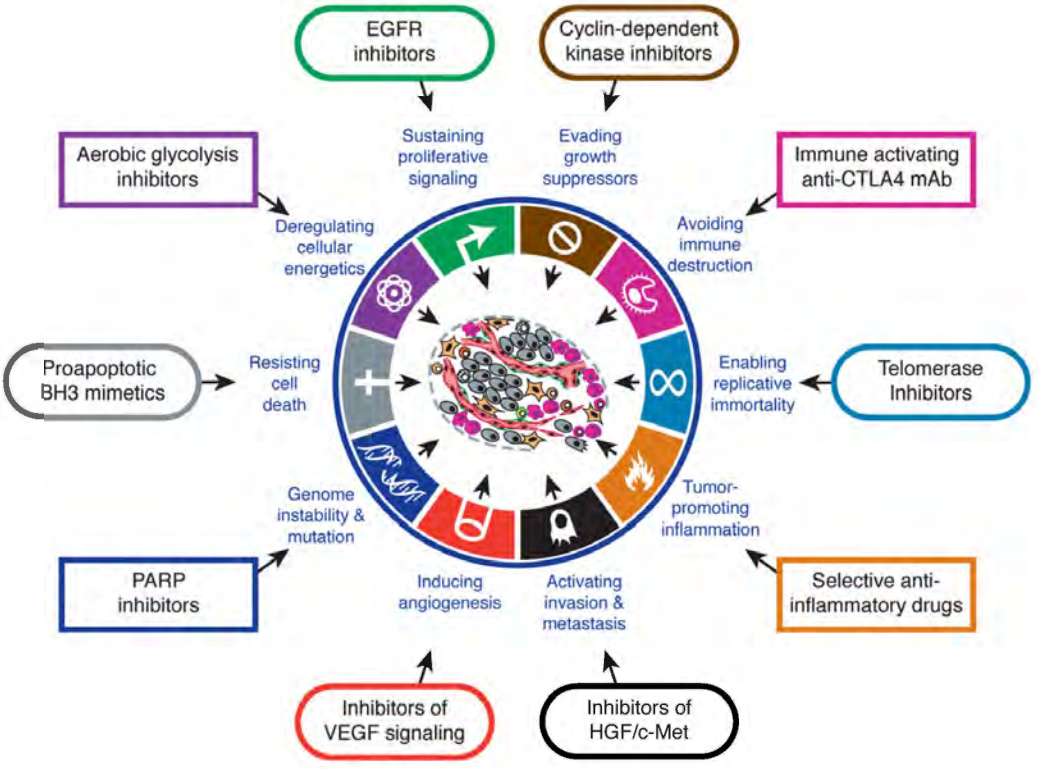
EGFR inhibitors
Cyclin-dependent kinase inhibitors
Sustaining proliferative signaling
Evading growth suppressors
Aerobic glycolysis inhibitors
Immune activating anti-CTLA4 mAb
Deregulating cellular energetics
Avoiding immune destruction
Proapoptotic BH3 mimetics
Resisting cell death
Enabling replicative immortality
Telomerase Inhibitors
Genome instability & mutation
Tumor-promoting inflammation
PARP inhibitors
Inducing angiogenesis
Activating invasion & metastasis
Selective anti-inflammatory drugs
Inhibitors of VEGF signaling
Inhibitors of HGF/c-Met

Minimum Noise Fraction: Automatic Band Selection

- Previous works include:
  - Manual inspection of Eigen-images
  - Automatic selection of Eigen-images based on its RMSE error to a clear image [$]
  - Computationally expensive
  - Time Consuming
- The optimal value of K can be determined from the diagonal entries of $\Lambda_{MNF} = SNR + 1$
- The Rose criteria [&] states that an SNR of at least 5.0 is needed to be able to distinguish image features at 100% certainty.

Algorithm 1 MNF($Y \in \mathbb{R}^{N \times S}$)

1: Estimate Data Covariance Matrix: $\Sigma_Y = Cov\{Y\}$
2: If δ is unknown, estimate: $\delta \sim Y(j,:) - Y(j+1,:), \forall j = 1 : N-1$
3: Estimate Noise Covariance Matrix: $\Sigma_\delta = \frac{1}{2} Cov\{\delta\}$
4: Calculate MNF projection vectors: $(\Sigma_Y \Sigma_\delta^{-1})\Phi = \Lambda_{MNF}\Phi$
5: Project data along MNF vectors: $Y_{MNF} \in \mathbb{R}^{N \times S} = Y\Phi$
6: Initialize $R \in \mathbb{R}^{S \times S}$ as top rank-K matrix
7: Project data back: $D \in \mathbb{R}^{N \times S} = Y_{MNF} R(\Phi^{-1}) = Y\Phi R(\Phi^{-1})$

[$] Reddy, K., and Bhargava, R. "Accurate histopathology from low signal-to-noise ratio spectroscopic imaging data." Analyst 135.11 (2010): 2818-2825.
[&] Bushberg et al. "The essential physics of medical imaging". Lippincott Williams & Wilkins, 2011.

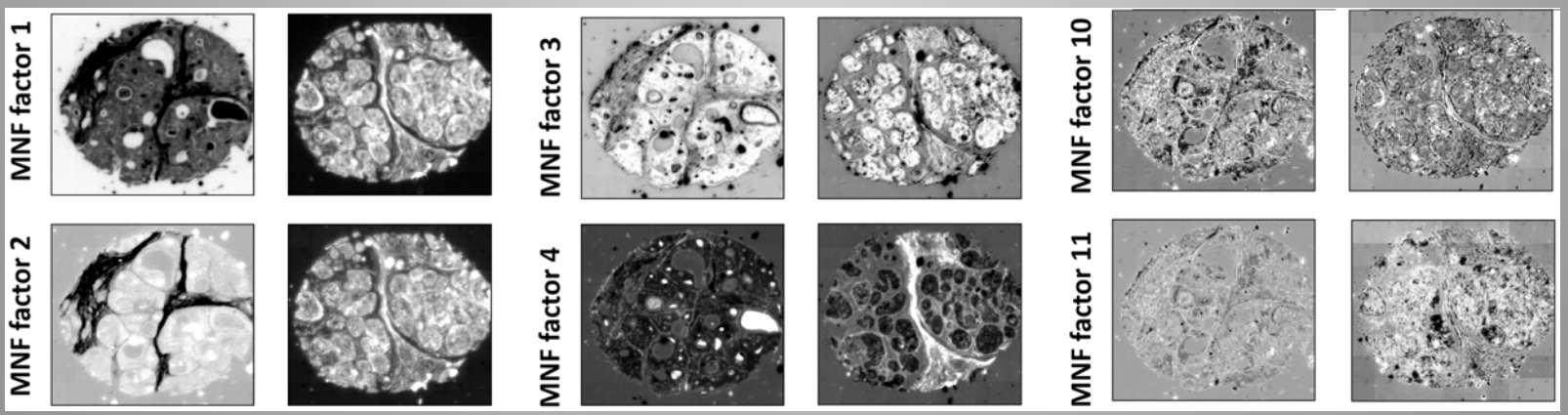

Blind Error Metric

- Absence of ground truth
- The Method Noise Image (MNI)*
  - No-reference metric, simple and easy to use
  - Based on Structural Similarity Index Metric% (SSIM)
  - Scores based on intensity, contrast, Image moments
  - Maximum score around highly structured regions

Algorithm 4 MNI Metric $(I, \hat{I})$

1: **Input**:
2: Noisy Image I, Denoised Image $\hat{I}$
3: **Body**:
4: Compute difference image $\hat{I}$: $M = I - \hat{I}$
5: Compute $SSM_P = SSIM(I, M)$
6: Compute $SSM_Q = SSIM(\hat{I}, I)$
7: Compute image quality score $e = Corr(SSM_Q, SSM_P)$

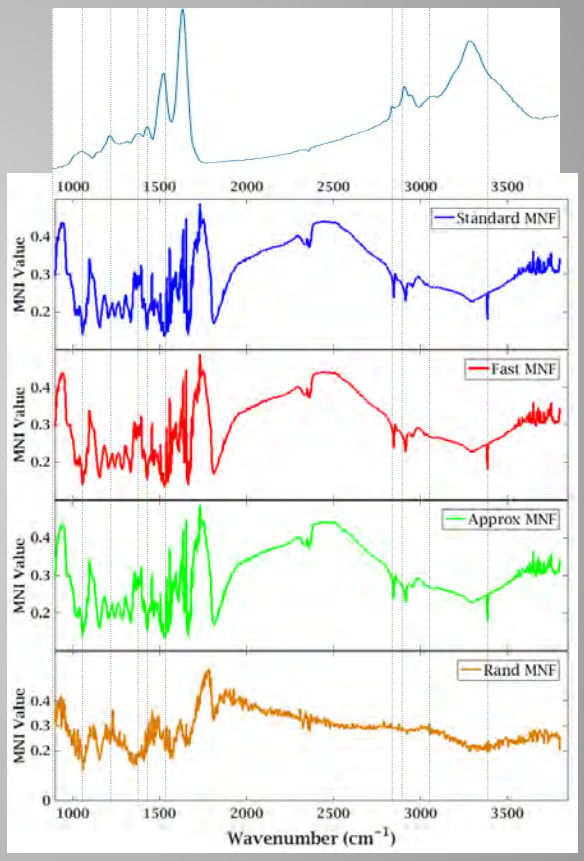

* Kong, Xiangfei, et al. "A new image quality metric for image auto-denoising." Proceedings of the IEEE International Conference on Computer Vision. 2013.
% Wang, Zhou, et al. "Image quality assessment: from error visibility to structural similarity." IEEE transactions on image processing 13.4 (2004): 600-612.